Glass and Glass–Ceramic Photonic Materials for Sensors

(Article begins on next page)

08 November 2022

Glass and glass-ceramic photonic materials for sensors

Matteo Giardino[1][0000-0003-1492-2498], Diego Pugliese[1][0000-0002-6431-1655] and Davide Janner[1][0000-0001-7954-979X]

[1] Dipartimento di Scienza Applicata e Tecnologia (DISAT) and RU INSTM, Politecnico di Torino, Torino 10129, Italy
davide.janner@polito.it

Abstract. Recent developments in sensors are pushing for optimized materials that can increase their usage, bolster their sensitivity and enable new and more efficient transduction mechanisms. We hereby review some of the most relevant applications of glasses and glass-ceramics for photonic sensors considering the recent trends and innovative approaches. This review covers from bulk glasses to thin films and from fiber optics to nanocrystal-based and their applications in sensing.

Keywords: Sensors, Nanoparticles, Photonics, Thin Films, Waveguides.

Table of content

1 Introduction

With the development of technology and its pervasive implementation in all aspects of modern life, all fields are experiencing a "smart" revolution where (artificial) intelligence and feedback system are required for an ever-increasing number of products and services. The extension of this revolution covers public services and natural resources, e.g., smart cities, capillary monitoring devices, and low-cost implementation of control points. That drives the development of sensors able to measure many different parameters that later can be used for the algorithms/control systems as feedback. In this scenario, sensors are developing steadily, and particularly, photonics-based sensors are attracting interest because of their high sensitivity, immunity to electromagnetic radiations, and small form factor. A key role in photonic sensors' development is assumed by selecting the more suitable optical materials to be employed. Indeed, if traditional bulk materials are well known and widely used, new materials and nano-/micro-structured ones can boost the performance of photonic sensors contributing to broader adoption and more capillary network sensors implementation. Among the different photonic materials used, glasses and glass-ceramics are of great interest because of their optical properties (particularly for oxides). Although a vast knowledge base is available for these different materials [1–5], there is still room for improvement. This work will give an overview of glass/glass-ceramic materials of interest for sensing and their application. The following sections will cover three main topics: bulk materials and thin films, fiber optics and fiber Bragg grating sensors, application of nanomaterials as sensing platforms.

2 Bulk materials and thin film-based sensors

Photonic bulk materials can be used for sensing and detectors either as macroscopic pieces or in the form of thin films where waveguiding mechanisms can also be exploited. In the following, two main applications of those types of materials are considered: scintillation in bulk materials and thin film-based sensors.

2.1 Scintillation

Scintillators are defined as a class of materials that emit light when excited by ionizing radiations. Their applications include the detection of neutrons, X-rays, gamma-rays, alpha-particle, and beta-particles.

The physical process of scintillation can be essentially divided into three steps, as sketched in Fig. 1 [6]:

- Conversion: the energy of the radiation impacting the material can excite electrons and generate a significant number of electron-hole pairs. Since the ionization energy of an atom is usually in the range 5-20 eV,

whereas the photon of the ionizing radiations can have an energy ranging from 10 keV (X-rays) to more than 1 MeV (gamma rays), after ionization, there is an energy transfer to the electron in the form of kinetic energy.

- Transport: the electron-hole pairs can move through the material, and, during this step, they can be trapped in the defects of the materials. This trapping leads to a significant loss in their energy and a delay in the emission process.

- Luminescence: the electrons and holes can also be trapped in a luminescence center. These luminescence centers can originate from some intrinsic defects of the material or an included element added for that aim. Light emission originates from the radiative recombination of the electron-hole pair. In some cases, the emission process may also involve the energy transfer from a sensitizer.
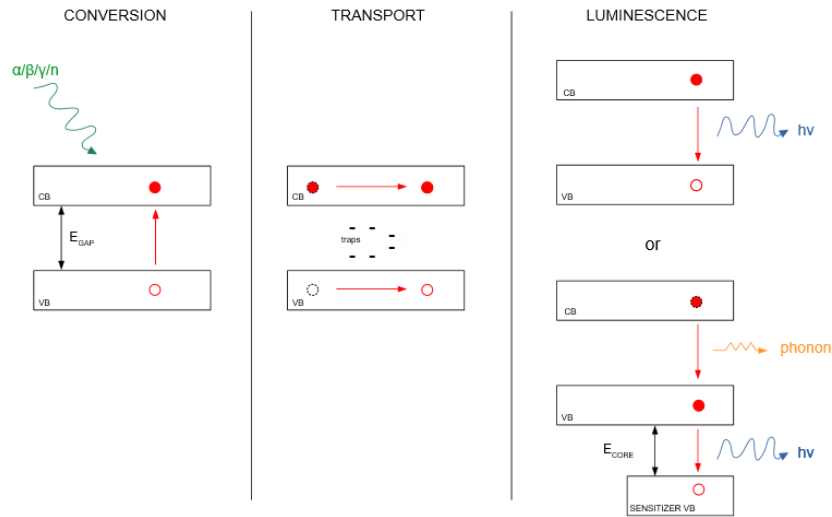
Fig. 1. Schematization of the three steps involved in the scintillation process.

The excited electron may also decay in a nonradiative mode by transferring its energy to the bulk matrix through vibrations (phonons). If the energy surplus of the excited electron is much greater than the maximum phonon energy of the material, the system's relaxation requires a multiphonon decay, and the scintillating efficiency of the glass is reduced [7].

Rare-earth halides, such as CeBr, $LaCl_3Ce$, and LuI_3Ce are among the compounds with higher scintillation yield but are hygroscopic, exhibit fair mechanical properties, and require expensive production processes [8].

For these reasons, the scintillating properties of halides nano-/micro-crystal embedded in glass-ceramic matrixes have been extensively explored in the last two decades and give a promising perspective to the field.

The material obtained by the inclusion of halides nano/micro-crystals in a glass matrix shows all the properties of a glass-ceramic system such as mechanical strength, chemical resistance, and thermal stability with low phonon energy, which results in a low probability of nonradiative recombination while retaining a good efficiency in the conversion. Moreover, impurity elements in the glass matrix are usually a fundamental requirement to obtain a scintillating behavior, and some dopants, e.g., Ce^{3+}, Pr^{3+}, Gd^{3+}, and Tb^{3+}, may also be added to increase the scintillation efficiency of the glass system.

Scintillating glasses are usually prepared by melt-quenching or by sol-gel process.

Struebing et al. [9] reported on a neutron scintillator glass-ceramic system by incorporating CaF_2:Eu nanocrystal in a glass matrix containing some ^6Li whose role is to increase the neutron absorption cross-section of the glass-ceramic scintillator (GCS). This system demonstrated a much higher scintillation efficiency than the glass matrix, and this enhancement is likely due to the more efficient energy transfer from the CaF2 nanocrystals to the Eu3+ ions that act as emitting centers.

Zheng et al. [10] produced Tb^{3+}-doped $BaGdF_5$ glass-ceramics for X-ray detection, showing a very high scintillation efficiency. The Tb^{3+}-doped glass-ceramics with composition $17SiO_2–11H_3BO_3–10Al_2O_3–6Cs_2CO_3–32BaF_2–17GdF_3–7TbF_3$ (mol%) was produced by melt-quenching technique, and the study compared the performance of this glass system before and after the thermal treatment. They reported emissions of the glass-ceramic at 274 nm and 377 nm excitation, respectively, 1.4 and 3.1 times stronger than that of the glass sample.

Khang et al. [11] added $GdBr_3$ and $CeBr_3$ to a crystalline phase in a silica-alumina glass matrix to obtain a detector for application in nuclear spectroscopy and gamma-ray detection. They observed an emission peak at 410 nm, which is a higher wavelength than the emission peak of traditional Ce^{3+}-doped silica glasses, and this wavelength shift is likely to be caused by the presence of Gd-rich nanoclusters. As reported in Fig. 2, this device also responds to α particles from ^{241}Am, β particles from $^{90}Sr/^{90}Y$, and neutrons from ^{239}Pu/Be source.
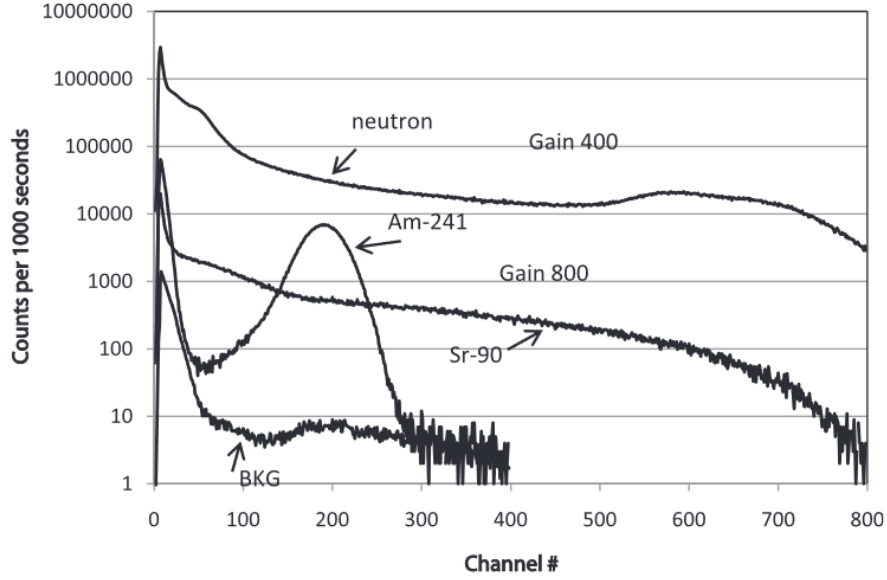
Fig. 2. Spectra of the glass-matrix detector for ^{241}Am alpha particles, ^{90}Sr/^{90}Y beta particles, and radiation background at gain 800 and for a ^{239}Pu/Be neutron source at gain 400. Reproduced from [11]. Copyright 2013, with permission from Elsevier.

2.2   Waveguides in glasses

When a light ray strikes at the interface between two media, with an incidence angle θ_i , refraction occurs, and the ray continues its propagation with a refraction angle θ_r given by Snell's law:

$$n_1 \, sin \, \theta_i = n_2 sin \, \theta_r \tag{1}$$

where n_1 and n_2 are the refractive indexes, respectively, of the first and second medium.

When $\sin \theta_r$ is equal to 1, i.e., the refraction angle assumes the critical value $\frac{\pi}{2}$, there is no longer a refraction wave, and the ray is completely reflected. This situation, represented in Fig. 3 and called ***total internal reflection (TIR)***, always occurs when the incidence angle is equal or greater than a critical value θ_i^{cr} given as:

$$\theta_i^{cr} = asin \left(\frac{n_2}{n_1} \right) \tag{2}$$

From   (4), it is clear that the TIR phenomenon only takes place when a light ray impinges the boundary of a medium with a lower refractive index because, according to the codomain of sin function, the ratio $\frac{n_2}{n_1}$ must always be lower than or

equal to 1 and that means that n_1 must be greater than or equal to n_2. The case $n_1 = n_2$ is also excluded since it would entail that θ_i is equal to θ_r , and no refraction would be observed.

When a light ray is "forced" to propagate in a medium surrounded by another one with a lower refractive index, a so-called waveguide is obtained by exploiting the total internal reflection phenomenon.

Many configurations may be used to obtain these waveguides, although this paragraph mainly focuses on *planar waveguides,* whereas Section 3 deals more in detail with *optical fiber*s.

The propagation of the light into the waveguide can be affected by the external environment, and this mechanism can be exploited for sensing purposes. Indeed, the sensors so obtained can be classified under four main categories according to which feature of the light is affected by the external environment. These four categories of sensing mechanisms are: intensity-modulation, phase-modulation, polarization-modulation, and wavelength-modulation.
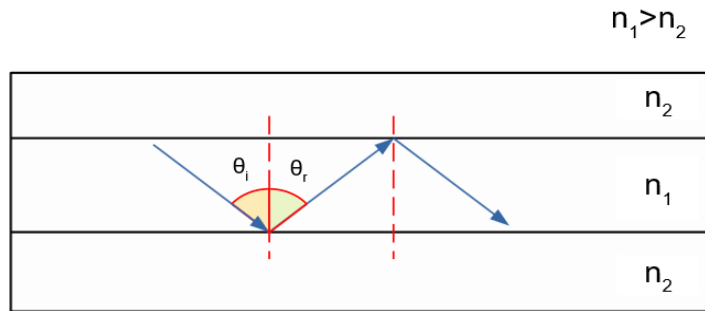

Fig. 3. Illustration of total internal reflection phenomenon in a planar waveguide.

To obtain a waveguide, one can start from a planar sample and must produce a variation of the refractive index on its surface.

The refractive index variation is obtainable either by creating a change in the chemical composition of the material or introducing some stresses into the material [12].

As far as glasses are concerned, one of the possible *glass waveguide (GWG)* fabrication methods is the *ion-exchange technique*. The latter consists of immersing the glass in a molten solution of a salt, usually a nitrate.

Walker et al. [13] performed an Ag^+ exchange by immersing a masked soda-lime glass into a molten $AgNO_3$ bath, obtaining a refractive index variation on the surface of 0.09. Moreover, K^+ turned out to be an excellent alternative to Ag^+ for waveguides fabrication by ion exchange [14]. It is worth underlining that by this technique, pretty thick modified layers can be obtained: Giallorenzi et al. [15] treated a soda-lime glass in a KNO_3 bath at 365 °C for 24 h and obtained a K^+ substituted layer with a thickness of around 8 µm, as shown in Fig. 4.
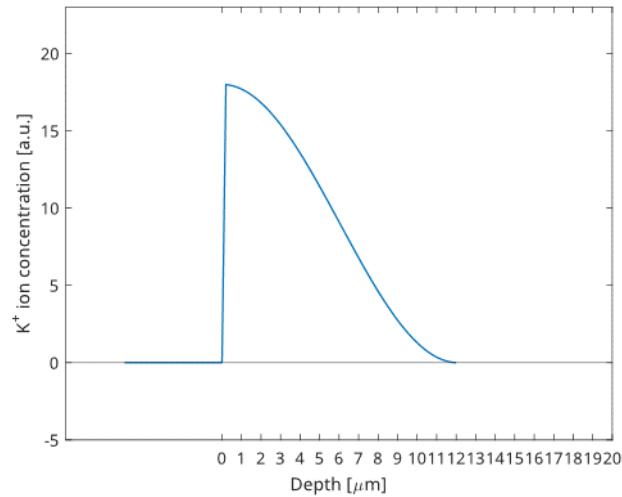
Fig. 4. Ion concentration profile, as a function of the depth, in a soda-lime glass treated for 24 h in a molten KNO_3 bath at 365 °C. Adapted from [15].

On the other side, GWGs can also be produced by depositing a thin film of a suitable material having a different refractive index (RI) on a glass substrate. The thin-film deposition can be realized in a plethora of different ways, including radio-frequency (RF) sputtering, pulsed-laser deposition (PLD), chemical vapor deposition (CVD), or even sol-gel processes. Despite being a much slower process and showing limits on the maximum achievable thickness, sputtering and CVD allow obtaining more uniform and higher quality thin films and the deposition of complex composition layers.

Chiasera et al. [16] proposed SiO_2-P_2O_5-HfO_2-Al_2O_3-Na_2O glasses activated by Er^{3+} ions obtained by multitarget RF sputtering. In particular, they produced a GWG by sputtering a SiO_2 target onto a disk of a $69P_2O_5$-$15SiO_2$-$10Al_2O_3$-$5Na_2O$-$1Er_2O$ glass, and one of HfO_2 was positioned.

On the other hand, the sol-gel process is a quick and inexpensive way of depositing thin optical films on flat substrates by spin-coating.

Almeida et al. [17] realized, by a two-step sol-gel method, a co-doped Er^{3+}/Yb^{3+} sulfide glass. This glass was obtained by first depositing oxide gel films on a silica glass or borosilicate glass and then sulfidizing the oxide gel into a sulfide by exposure to H_2S gas in temperature.

In waveguide applications, also glass-ceramic materials have recently attracted noticeable attention. Indeed, *glass-ceramic waveguides (GCWGs)* can be obtained by appropriate thermal treatment to produce a phase separation. They typically show a sandwich structure where a glass layer is surrounded by another layer consisting of a crystalline phase dispersed into an amorphous matrix. Moreover, also rare-earth dopants are usually embedded in the form of nanocrystals, and an example of this approach is the GCWG by Jestin et al. [18], who proposed a SiO_2-HfO_2 activated by Er^{3+} GWG obtained via sol-gel route and subsequent dip-coating deposition onto a

SiO$_2$ substrate and annealing treatment at 900 °C. A high-resolution transmission electron microscopy (HRTEM) image of the synthesized silica-based glass-ceramic nanocomposite material is reported in Fig. 5.

In this case, the refractive index of the SiO$_2$-HfO$_2$ film can be finely tuned by controlling the HfO$_2$ concentration and the annealing process parameters, which influence the composition and the phase separation of the glass-ceramic system.

Er^{3+} doping is often considered in GWCs and GCWGs since it displays a very strong emission at around 1500 nm [19], which is the wavelength where the silica glass shows the lowest loss (about 0.2 dB/km) and is, therefore, the most common for telecommunications purposes.

Optical waveguides are suitable for various sensing purposes in analytical chemistry, ranging from the detection of gases [20, 21] to the pH measurement of water solution [22, 23].

Han et al. [21] realized a spiral chalcogenide glass waveguide for methane detection to operate in the middle infrared region (MIR) and observed its transmittance T follows the Beer-Lambert law:

$$T = \exp\left(-\alpha L C\right)$$

(3)

where α is the absorption coefficient, L is the waveguide length, and C is the methane concentration.

The pH sensing, in particular, is usually accomplished by realizing a porous layer on the outer surface of the waveguide where a pH-sensitive dye can be incorporated.

Moreover, waveguides have also been successfully employed in biology to monitor the bacteria growth process [24]. In this case, the outer surface of the waveguide is often functionalized with an antibody that can bind certain bacteria so that a change in the refractive index is observed close to the surface and can be probed employing an evanescent wave.
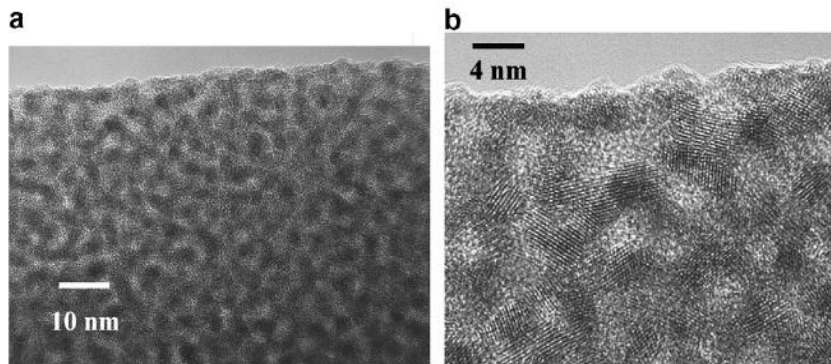
Fig. 5. HRTEM image of SiO$_2$-HfO$_2$ thin film at different magnifications. Reproduced from [18]. Copyright 2007, with permission from Elsevier.

2.3 Thin films for sensing

A wide range of oxide thin film (OTF) sensors has been prepared on glass substrates by deposition, with different techniques.

The first OTF sensor for gas detection was proposed in 1962 by Seiyama et al. [25] and was based on the steep electrical conductivity variations that occur when a gas adsorbs or desorbs from a porous semiconductor layer at high temperature. This thin film was deposited onto a borosilicate glass by evaporating a thin layer of metallic Zn which was subsequently oxidated in the air at 450 °C for 10 h.

Although Seiyama's work focused only on a ZnO layer [25], also many other semiconductor metal oxides, such as TiO_2, WO_2, In_2O_3, and SnO_2, have been employed for the preparation of gas thin film-based sensors due to the considerable variation in their conductivity when exposed to chemical vapor.

The sensor has been tested by exposing it to different CO, benzene, toluene, and propane concentrations while its increase in electrical resistivity has been recorded over time. This increase is due to the absorption of the above-mentioned organic molecules which behave as electron donors to the ZnO (n-type doping).

The thin film-based sensors are mainly composed of a porous metal oxide semiconductor thin layer deposited on a glass substrate through different techniques.

Among the techniques commonly employed, it is worth mentioning physical vapor deposition (PVD), laser ablation, molecular beam epitaxy, sputtering, chemical vapor deposition (CVD), sol-gel techniques, and ultrasonic spray pyrolysis spin, and dip-coating.

Touidjen et al. [26] deposited a SnO_2 thin film on a glass substrate to realize an organic vapor sensor that successfully detected ethanol vapor in the concentration of a few dozen ppm. The deposition was performed using spray-pyrolysis techniques using an isopropanol-aqueous $SnCl_2$ solution as a precursor.

Salman et al. [27] deposited a TiO_2:Mn thin film utilizing RF sputtering with a pure TiO_2 target on an Indium-Tin Oxide (ITO) glass and subsequent annealing thermal treatment at 600 °C.

Salah et al. [28] exploited the spin-coating of a ZnO sol which was prepared using zinc acetate, 2-methoxyethanol, and ethanolamine on a glass substrate to work as a humidity sensor in the range 15-95 relative humidity (RH%). The sensor is based on the electrical resistance decrease when water molecules chemisorb or physisorb (especially at high RH% values) on the ZnO surface.

Glassy thin films are also employed for sensing applications. A remarkable example is represented by chalcogenide glasses-based thin-film, which have been extensively investigated over the years, as materials for producing membranes for potentiometric techniques of heavy metal ions (e.g., Fe^{2+}, Cu^{2+}, Pb^{2+}, Ag^+) in water or even as pH sensor [29]. The probe obtained was tested as an electrode in an electrochemical cell with a double liquid junction, and cell voltage was plotted against the Pb^{2+} ion concentration as reported in Fig. 6.
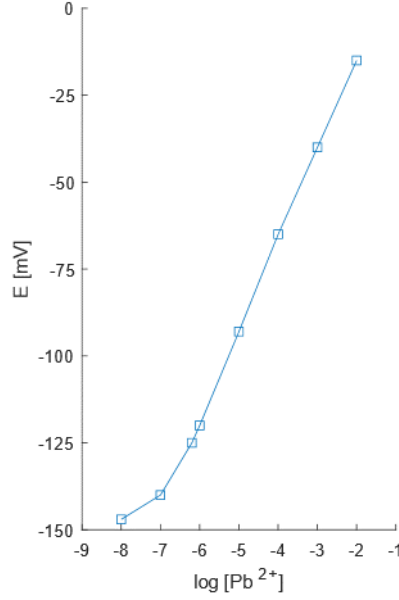
Fig. 6. Calibration curve of a chalcogenide glass thin film sensor for quantification of Pb^{2+} ions in water. Adapted from [29].

In the field of thin films for sensing, even metallic glasses (MGs) find a plethora of different applications.

Metallic glasses are usually produced by extremely rapid cooling of a molten alloy so that the metallic system solidifies without crystallizing but rather forming an amorphous structure similar to traditional glasses.

This category of materials demonstrates excellent flexibility and elasticity, high chemical resistance due to the lack of grain boundaries, high electrical conductivity, and provides good adhesion to the other layers. Moreover, since diffusion via grain boundary mechanism is not allowed, it is possible to realize a diffusion barrier to prevent interdiffusion at the interface. Also, electron scattering and current leakage are minimized by the MG's grain-free structure, limiting the electron scattering [30].

MGTF may show a piezoresistance effect [31] and can thus be used as a strain sensor. Piezoresistance is a change of the electrical resistance of a material when a mechanical deformation is applied, typically due to the change of interatomic distance, which affects the bandgap.

Since the electrical resistance vs. strain dependence in MGTF is usually linear, this behavior is described by introducing a gauge factor (GF) which may be defined as the ratio between the relative variation of resistance and the strain:

$$GF = \frac{R - R_0}{\varepsilon R_0} = \frac{\delta R}{\varepsilon} \tag{4}$$

Xian et al. [31] proposed the metallic glass system $Zr_{55}Cu_{30}Ni_5Al_{10}$ to be deposited as a thin film by ion beam sputtering on a polycarbonate substrate to create an e-skin sensor and observed a GF of 2.86. In Fig. 7, the normalized electrical resistance variation $\Delta R/R_0$ vs. the strain for this MG system is reported.

A different approach that uses pyro-resistivity of a graphene layer deposited on top of $LiNbO_3$ has been reported in [32]. In that device, light is shone on the ceramic material that changes its temperature due light absorption and charge formation on the surface. Those charges dope the graphene layer that changes its resistivity and can be interrogated electrically. In this way, a broadband detector is realized and shows good performance in terms of detectivity, even in the mid-infrared spectral region.
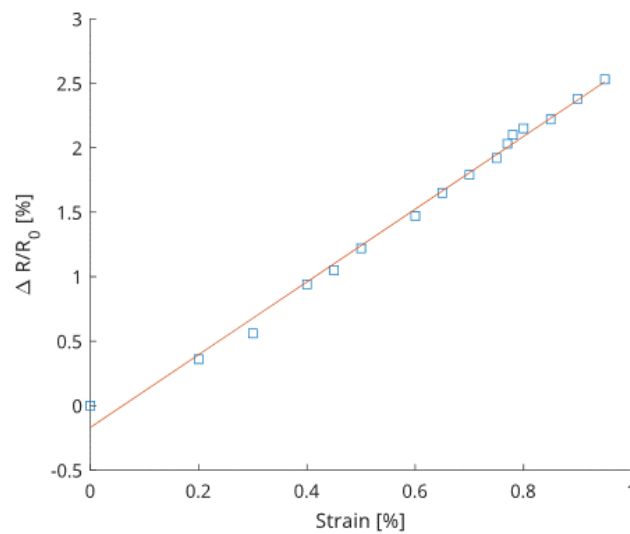
Fig. 7. Dependence of relative resistivity vs. applied strain of a $Zr_{55}Cu_{30}Ni_5Al_{10}$ thin film metallic glass. Adapted from [31].

3 Fiber optics-based sensors

Among the approaches that leverage glasses for sensing, fiber optics-based sensors are among the most promising in terms of flexibility, ease of use, and integration. The primary sensing mechanisms in this type of sensor are based on the change in the light propagation in the fiber when the surrounding environment changes. Thus, they share many features in common with the waveguide sensor presented above. However, for their peculiarities and widespread use, the following Section is entirely dedicated to this type of sensors covering the most common configurations for sensing and the glass/glass-ceramic materials used in these applications.

12

3.1 Gratings-based sensors

Among the different optical fiber sensors, Fiber Bragg Gratings (FBGs) are the most widespread. Indeed, they show many interesting features like high sensitivity, and they work at a particular wavelength allowing for multiplexing a high number of sensors along with the same fiber [33]. Moreover, their fabrication is relatively cheap, and their sensitivity can be significantly increased by adding a layer of a polymeric or glass/ceramic material around the fiber [3, 33].

An FBG is a distributed Bragg reflector in a fiber reflecting specific wavelengths of light, typically around 1550 nm. This mechanism is obtained by introducing a periodic variation of the refractive index inside the fiber optics with a periodicity proportional to the Bragg wavelength at which the reflection occurs, as indicated schematically in Fig. 8.
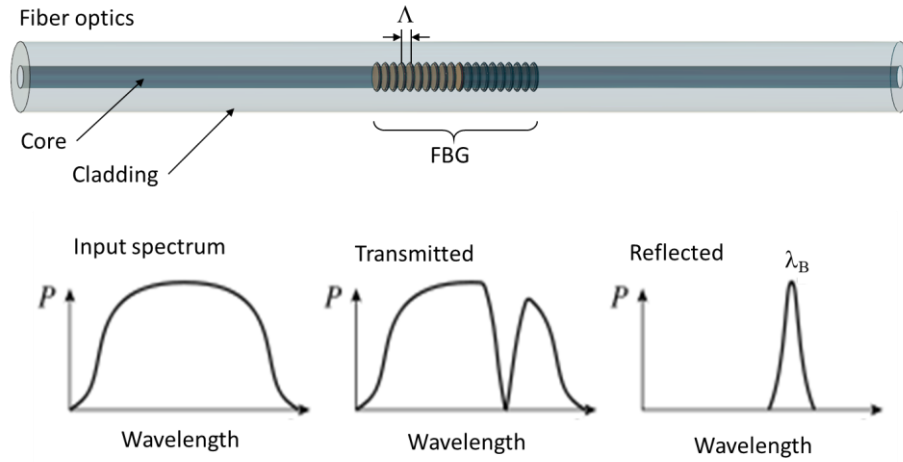
Fig. 8. Periodic index variation of period Λ in the core of a fiber optics and its spectral response in transmission and reflection showing the relationship between Λ and the peak wavelength λ_B.

The refractive index variation is typically of the order of 10^{-4}-10^{-2}, and the area affected by such modification ranges from 3 to 10 mm [33]. The index variation is obtained in the fiber core by the formation of color centers or physical damage according to the technique used but always relying on laser irradiation (either ultraviolet or femtosecond). The Bragg wavelength λ_B is related to the refractive index n_f of the fiber and the periodicity Λ of the modification as follows:

$$\lambda_B = 2\, n_f \Lambda$$

(5)

The primary sensing mechanisms for FBG can rely on three refractive index modification phenomena: temperature, strain, and refractive index change around the fiber. While the first two are present in all types of FBG, the last one is only affecting special types of FBG like etched cladding or tilted ones [4, 33]. An example of sensing

application with FBG can be found in harsh environments like nuclear sensing [34]. In that case, FBGs have been used to monitor the temperature in a radioactive environment, and the fiber was encapsulated with a special ceramic coating ORMOCER® demonstrating the ability to measure up to 450 ℃ keeping a tightly sealed environment. The advantage of fiber optics sensors is made evident in harsh environments, given their immunity to electromagnetic interference, the electric power-free operation of the sensor, and the possibility of interrogating it remotely with light propagating in the fiber.

To exploit the sensing mechanism based on refractometry in a fiber, tilted FBGs can be used [4]. As illustrated in Fig. 9a, a tilted FBG is a periodic variation of the index of refraction similar to FBG but tilted at an angle with respect to the propagation direction. The associated transmission spectrum (Fig. 9b) shows many dips related to modes of light that travel in the cladding of the optical fiber. Such cladding modes are sensitive to the environment refractive index and present a shift in wavelength upon its variation. This mechanism can be exploited for refractometric sensing by monitoring the wavelength and transmitted power of one of the dips, as exemplified in Fig. 9c.
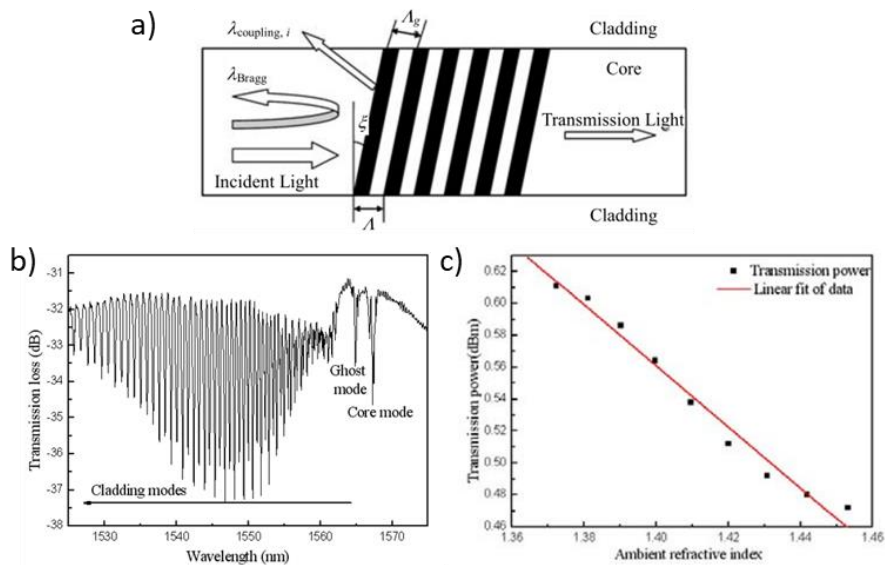
Fig. 9. a) Light scattering and transmission in a fiber with a tilted FBG. b) Optical spectral response of a tilted FBG. c) Dip power variation vs. external refractive index showing the sensing principle. Adapted from [35] with permission from the Institute of Electrical and Electronics Engineers.

Coating the exterior of the fiber with glass or glass-ceramic materials can significantly enhance the sensitivity of the sensor and make it more specifically sensitive to, e.g., humidity, pH, giving the possibility to target many different parameters to be measured. For instance, depositing a 200 nm coating of ITO greatly increases the sensing

performance in terms of sensitivity [36], making this sensor a good candidate for biochemical sensing after surface functionalization.

3.2 Lossy mode resonance

The integration of fiber optics with micro/nanotechnology has allowed the development of very sensitive photonic devices and fostered novel (bio-)sensing schemes [37]. Coating fibers with nanoparticles or nanofilms allows tailoring the optical features with an excellent spectral resolution, precision, and accuracy, enabling the realization of high-performance optical platforms [38, 39]. Indeed, the interaction of light traveling in a fiber optic with its surrounding environment can generate surface waves of different types, such as evanescent, Bloch, surface plasmon polariton, lossy/leaky mode, or derived from guided modes, etc. Many schemes can be used to excite those waves [40] and are sensitive to every change occurring in the medium surrounding the fiber [41], making them suitable for sensing applications. Among surface wave sensors, the deposition of metal-oxide nanofilms on fiber optics has allowed effective exploitation of lossy mode resonance (LMR) for sensing [42], attracting strong interest from many fields of applications. The basic principle of LMR sensors is illustrated in Fig. 10.
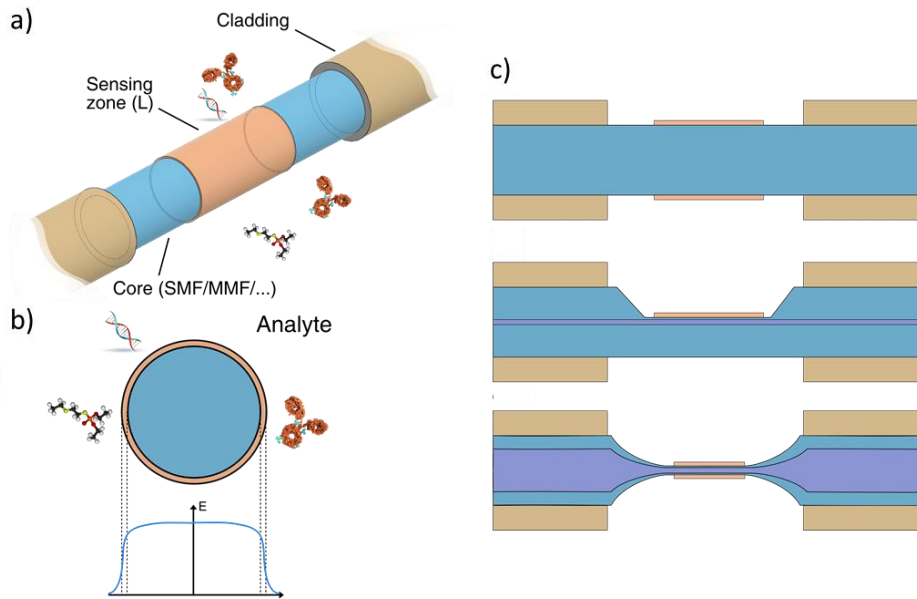
Fig. 10. Working principles of LMR. a) Sensing zone constituted by a thin film coating the fiber and interacting with b) the guided modes and the external environment (analyte). c) Possible configurations of LMR sensors showing the fiber optics and the sensing film. Adapted from [35] with permission from the Institute of Electrical and Electronics Engineers.

In a multimode fiber optic (MMF), the cladding is removed partially or completely, and the light propagating in the core is allowed to interact with the surrounding environment. As a result, refractive index variations are recorded as a change in the transmitted power at specific wavelengths. In addition, by coating the exposed core with glass/glass-ceramic material, the sensitivity can be significantly enhanced.

The complex (relative) permittivity of each material can be expressed as shown in (:

$$\varepsilon = \varepsilon' + j\varepsilon'' = Re\{\varepsilon\} + jIm\{\varepsilon\} = (n + jk)^2 \tag{6}$$

where ε' describes the lossless permittivity, whereas ε'' the lossy permittivity. The previous equation can also be rewritten in terms of n representing the material RI and k describing the extinction coefficient that refers to how strongly a substance absorbs light at a given wavelength. The selection of materials for sensitivity enhancement can be made using this parameter, and, in particular, dielectric materials with high RI (HRI) can be used in LMR. Indeed, many have been proposed [43], such as aluminum-doped zinc oxide (AZO), zinc oxide (ZnO), hafnium dioxide (HfO$_2$), zirconium dioxide (ZrO$_2$), tantalum oxide (Ta$_x$O$_y$), titanium dioxide (TiO$_2$), indium oxide (In$_2$O$_3$), indium gallium zinc oxide (IGZO), ITO, tin oxide (SnO$_{2-x}$), amorphous silicon, etc. Some complex HRIs (n,k) are shown in Fig. 11. At first glance, we see that no single material allows attaining the best performance, but the choice is application dependent, considering factors like the average RI of the environment and the operating wavelength of the device.

Moreover, n tends to decrease with the wavelength implying less LMR sensitivity, but conversely, the RI sensitivity increases at the same time. Therefore, a careful study and modeling of the device are compelling to design reliable sensors. So far, SnO$_2$ seems to guarantee the greatest performance in terms of RI sensitivity of LMR-based devices for RI ranges close to a water environment which is typical for, e.g., biosensing applications.

An example of a sensor obtained by LMR si reported in Fig. 12. The performance has been evaluated by considering two metal oxides, i.e., ITO and SnO$_2$, and two types of fibers, i.e., cladding-removed (CR)-MMF and side-polished (D-shaped) fiber. Fig. 12a and b illustrate the two types of sensors coated with thin films of ITO or SnO$_2$ and the experimental setups. Comparing the calibration curves (Fig. 12c), one can observe that, given the better optical features of SnO$_2$ (higher n, real part of permittivity; lower k, the imaginary part of permittivity), the best performance is achieved with D-shaped fibers. The optimized sensor features a SnO$_2$-coated ($\approx$160 nm) D-shaped fiber LMR biosensor, and its calibration curve based on Mouse IgG and goat anti-mouse-IgG is reported in Fig. 12d. Such device shows a limit of detection of 150 pg/L (1 fM), constituting, in terms of sensitivity, the best-performance biosensing platform in the literature so far.
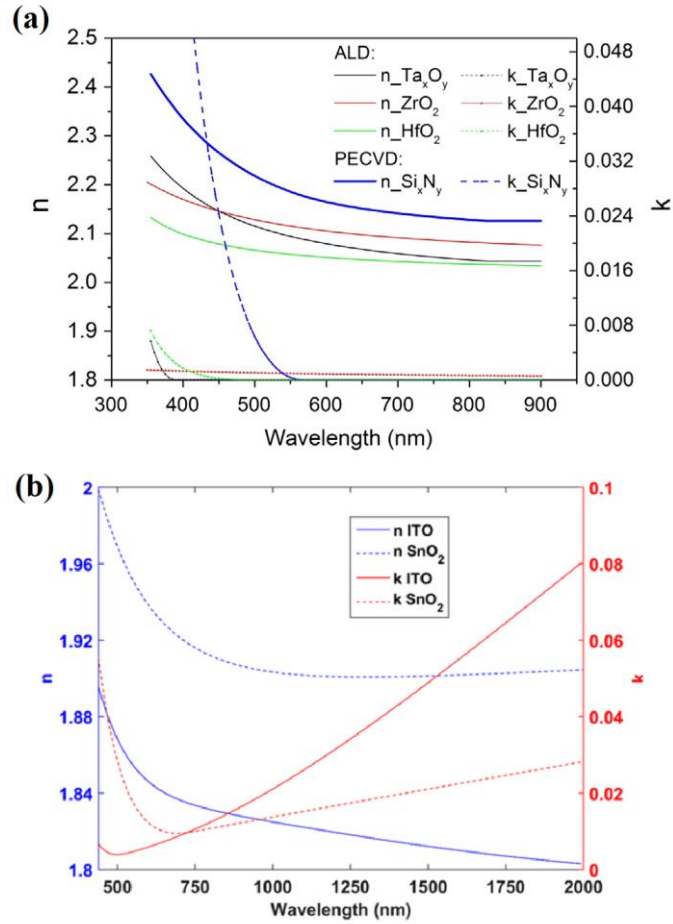
Fig. 11. (a) Dispersion characteristics in terms of *n* and *k* for HfO$_2$, ZrO$_2$, Ta$_x$O$_y$ deposited by atomic layer deposition technique and for SixNy films deposited by plasma-enhanced CVD. Adapted from [44]. Copyright 2018, with permission from Elsevier. (b) Dispersion characteristics in terms of *n* and *k* for ITO and SnO$_2$ deposited by direct current (DC) sputtering. Adapted from [43].
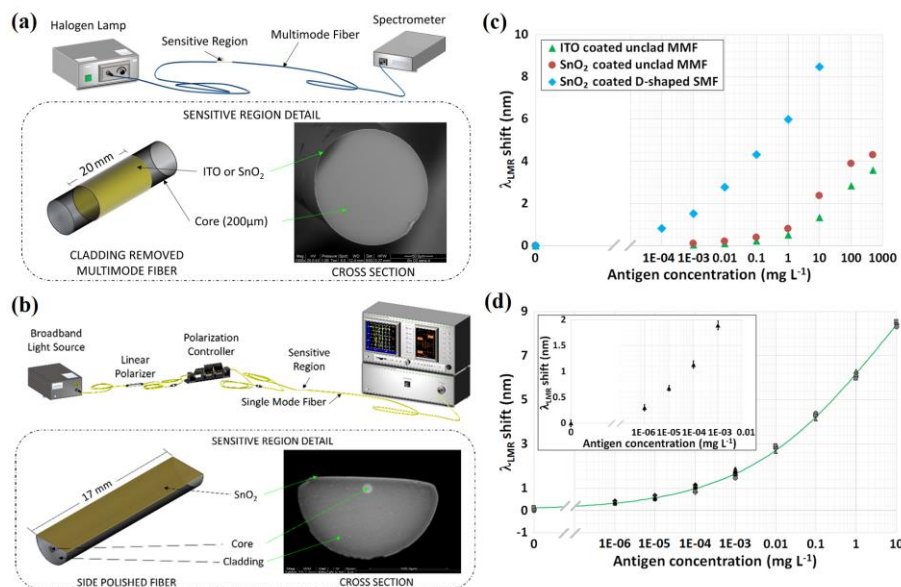
Fig. 12. (a) Scanning Electron Microscopy (SEM) image and a sketch of the sensing device consisting of CR-MMF coated with ITO or SnO_2, together with the experimental setup. (b) SEM image and sketch of the sensing device consisting of D-shaped single-mode fiber coated with SnO_2, together with the experimental setup. (c) Comparison of the calibration curves achieved with three LMR sensors: the ITO- (green triangles) and SnO_2-coated (red circles) CR-MMF biosensors, and the SnO_2-coated D-shaped single-mode fiber biosensor (sky blue rhombuses). (d) Calibration curve of the SnO_2-coated D-shaped biosensor repeated several times and displayed together with the sigmoidal fit of the experimental points. Adapted from [43].

4 Nanocrystals and quantum dots embedded glass-ceramics

The incorporation of nanocrystals and nanoparticles in a glass matrix allows enhancing its sensing properties.

On one side, nanocrystal glass-ceramics allows the realization of sensors based on the photon upconversion (UC) phenomenon, i.e. the process in which two or more photons, with a specific wavelength, are absorbed, causing the emission of photons with a shorter wavelength.

This UC-based sensor demonstrated a combination of unique properties, including photochemical and thermal stability, which make them the perfect candidate for the preparation of non-contact temperature probes.

On the other side, the embedding of quantum dots opens the door to realize a wide range of gas and chemical sensors due to their environment-sensitive fluorescence properties.

4.1   Nanocrystals

Trivalent rare-earth (RE) ions-doped UC materials have attracted a great deal of attention in the last decades due to their wide variety of applications in biological luminescent labels and drug delivery carriers, solar cells, all-solid-state UC lasers, and display devices [45–49].

Only more recently, luminescent UC materials, whose characteristic parameters including the absolute emission intensity, the fluorescence intensity ratio (FIR), the lifetime, and the peak wavelength could be strongly temperature-sensitive, have been profitably applied in the field of non-contact optical thermometry [50]. Notably, optical thermometry based on the FIR technique (see Fig. 13a) is recognized as one of the most valuable optical thermometry strategies due to its unique merits of contactless feature, fast response, simple data processing, and excellent resolution [51]. Moreover, the temperature-measurement FIR approach also displays some advantages over other optical-based techniques, such as fluorescence lifetime and amplified spontaneous emissions, in that much higher measurement accuracy and reliability could be achieved due to FIR being independent of external interferences, spectrum losses, and fluctuations in excitation density [52]. In light of all the above-mentioned promising features, this type of non-contact optical sensors can be used in many special environments, such as electrical transformer temperature in power stations, building fire detections, biological systems, and corrosive circumstances [53]; conventional contact-mode temperature sensors are not exploitable.

The research of high-performance FIR-based optical temperature sensors mainly focuses on optimizing active ions and the host matrix. Many RE ions, such as Pr^{3+}, Nd^{3+}, Sm^{3+}, Eu^{3+}, Dy^{3+}, Ho^{3+}, Tm^{3+}, Yb^{3+}, and Er^{3+} have been studied for temperature sensing based on the change of FIR of two thermally-coupled energy levels (TCELs) with temperature [54]. Er^{3+} ion is the most extensively investigated because of its intense UC luminescence and appropriate bandgap (around 800 cm^{-1}) between the $^2H_{11/2}$ and $^4S_{3/2}$ energy levels (see Fig. 13b), which exactly falls in the thermally coupled energy range (200–2000 cm^{-1}) [55]. To obtain stronger UC luminescence, Yb^{3+} is usually adopted as the preferred sensitizer for Er^{3+} due to its high absorption cross-section at 980 nm and efficient $Yb^{3+} \rightarrow Er^{3+}$ energy transfer efficiency [56]. Conversely, Yb^{3+} and Pr^{3+} are of less advantage due to slight energy differences, while Eu^{3+}, Ho^{3+}, and Tm^{3+} show energy differences above 1500 cm^{-1}, leading to thermal decoupling at low temperature [54].

Besides optimizing the RE active ions, the selection of a proper host material is also crucial for the application of UC materials in FIR-based temperature sensors. Host materials should exhibit low phonon energy for RE doping and good stability for long-term use, especially under the measured temperature range. In general, oxide materials show good physical and chemical stability. However, they have the shortcoming of high phonon energies, while fluoride materials can provide a low phonon energy environment for dopants and lead to efficient UC luminescence but are easy to undergo phase transformations at high temperatures [57]. Thus, novel materials combining the advantages of both oxide and fluoride materials should be a favorable host

for RE doping to achieve high-performance FIR-based optical temperature sensors with a good signal-to-noise ratio.
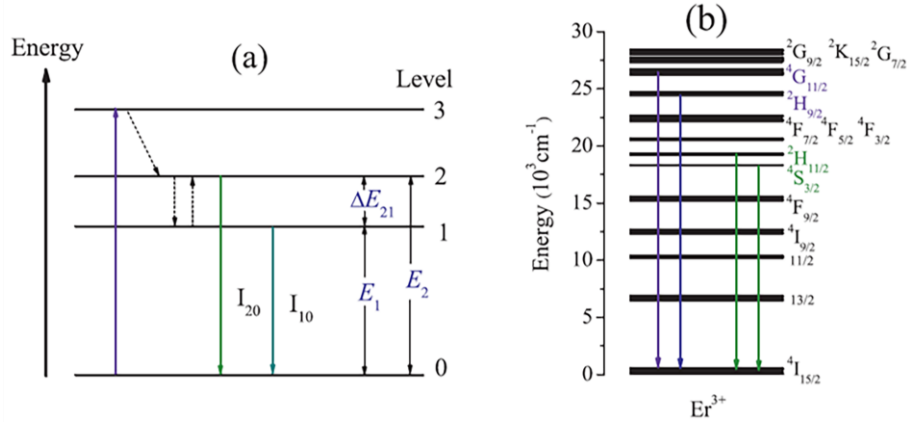
Fig. 13. (a) Schematic energy level diagram showing the energy levels and transitions of interest in the FIR-based optical thermometry technique; (b) energy levels of the Er^{3+} ions. Reproduced from [54]. Copyright 2014, with permission from Elsevier.

In this scenario, transparent oxyfluoride glass-ceramic (GC) luminescent materials, featured by the precipitation of fluoride nanocrystals (NCs) among the glassy oxide matrix with suitable chemical compositions, have attracted an increasing interest owing to their facile preparation and superb optical performance [52]. It is worth highlighting that incorporating the RE activators into the precipitated fluoride crystals with low phonon energy is of paramount importance to enhance luminescence in GC samples [58]. Moreover, compared to the powder and slice samples, where only the surface portions can be efficiently excited and emit due to the strong scattering of excitation/emission light, the optical properties of GCs may be markedly improved due to the "volume effect" of transparent material, i.e., the incident and output light can pass through the whole sample [59, 60]. Conventionally, GCs are formed through a finely controlled post-heat treatment of the glass at two different temperatures, firstly to induce nucleation and allow crystal growth of the nuclei [61]. Only more recently, femtosecond laser irradiation at a high repetition rate has been recognized as a powerful alternative technique to induce the precipitation of NCs only in spatially selected regions of the glass [62].

Interesting studies on the optical temperature sensing behavior of RE ions-doped transparent oxyfluoride GCs have been reported in the literature. Transparent GCs containing 25 nm-sized $NaYF_4$:Yb^{3+}/Er^{3+} crystals were successfully fabricated by S. Jiang et al. [54] and showed highly enhanced green UC emissions. The FIR of the two green UC emission bands corresponding to the $^2H_{11/2}$ and $^4S_{3/2}$ multiplets to the $^4I_{15/2}$ ground multiplet transitions was characterized for optical thermometry ranging from 298 to 693 K, and relative temperature sensitivity of 1.24 %K^{-1} at around 300 K was obtained.

Highly transparent bulk NaY_2F_7:Yb^{3+}/Tm^{3+} GCs with excellent temperature sensing performances, benefiting from the large energy gap of Tm^{3+} between TCELs of $^3F_{2,3}$ and $^1G_4$, were reported by S.Y.Z. Chen et al. [57]. In particular, the maximal relative and absolute sensitivity reached 1.63 and 10.01 %K^{-1} at 415 and 567 K, respectively.

Transparent oxyfluoride GC containing Yb^{3+}/Tm^{3+}/Er^{3+}:YF_3 nanocrystals was successfully synthesized by D. Chen et al. [52], and its potential application in FIR-based optical thermometry was systematically investigated. As a result, dual-modal temperature sensing was achieved with the assistance of FIRs of two emission bands between Er^{3+}:$^2H_{11/2} \rightarrow {}^4I_{15/2}$ and Er^{3+}:$^4S_{3/2} \rightarrow {}^4I_{15/2}$ as well as between Tm^{3+}:$^3F_{2,3} \rightarrow {}^3H_6$ and the combined Tm^{3+}:$^1G_4 \rightarrow {}^3F_4$/$Er^{3+}$:$^4F_{9/2} \rightarrow {}^4I_{15/2}$, showing maximal temperature sensitivities of 1.01 and 1.89 %K^{-1} at 293 and 393 K, respectively.

Transparent oxyfluoride GCs containing hexagonal $NaGdF_4$:Yb^{3+}/Ho^{3+} nanocrystals were fabricated by X. Li et al. [50] through the melt-quenching method followed by self-crystallization. The FIR of two blue UC emission bands peaked at 446 and 484 nm, originating from the transitions from two TCELs of $^5F_1$/$^5G_6$ and $^5F_{2,3}$/$^3K_8$ states to the $^5I_8$ state, was recorded for optical thermometry in the temperature range of 390 to 773 K and relative sensitivity of 1.43 %K^{-1} at 390 K, corresponding to an effective energy gap of 1515 cm^{-1}, was achieved.

4.2 Quantum dots

Quantum dots (QDs) are semiconductor particles whose dimensions are in the range of few nanometers (less than 10 nm) along all three spatial dimensions and are therefore usually referred to as zero-dimensional (0D) materials.

The typical band structure of QDs, compared to that of bulk semiconductors and single molecules, is reported in Fig. 14a.

As bulk semiconductor materials, a quantum dots can absorb a photon when an electron is promoted from the valence band to the conducting band, leaving a hole in the former, as shown in Fig. 14b. Consequently, it can emit radiation when the electron-hole pair gives rise to recombination through a radiative pathway.

When the sizes of the particles are in the order of magnitude of the size of the electron-hole pair, known as Bohr's radius, a quantum effect named quantum confinement is observed.

A very naive, but at the same time effective, way to explain the quantum confinement is to choose the particle in a one-dimensional (1D) box model.

Imagining that the electron is confined in a potential well, represented by the physical boundary of the QDs and solving the Schrodinger's equation under these conditions, the energy spectra of the particle itself can be expressed as:

$$\varepsilon_i = \frac{\hbar \pi^2}{2 m_e a^2} i \qquad i = 1,2,3,....$$ (7)

where $\hbar$ is the reduced Planck's constant, m_e is the effective mass of the electron, and a is the size of the quantum well.
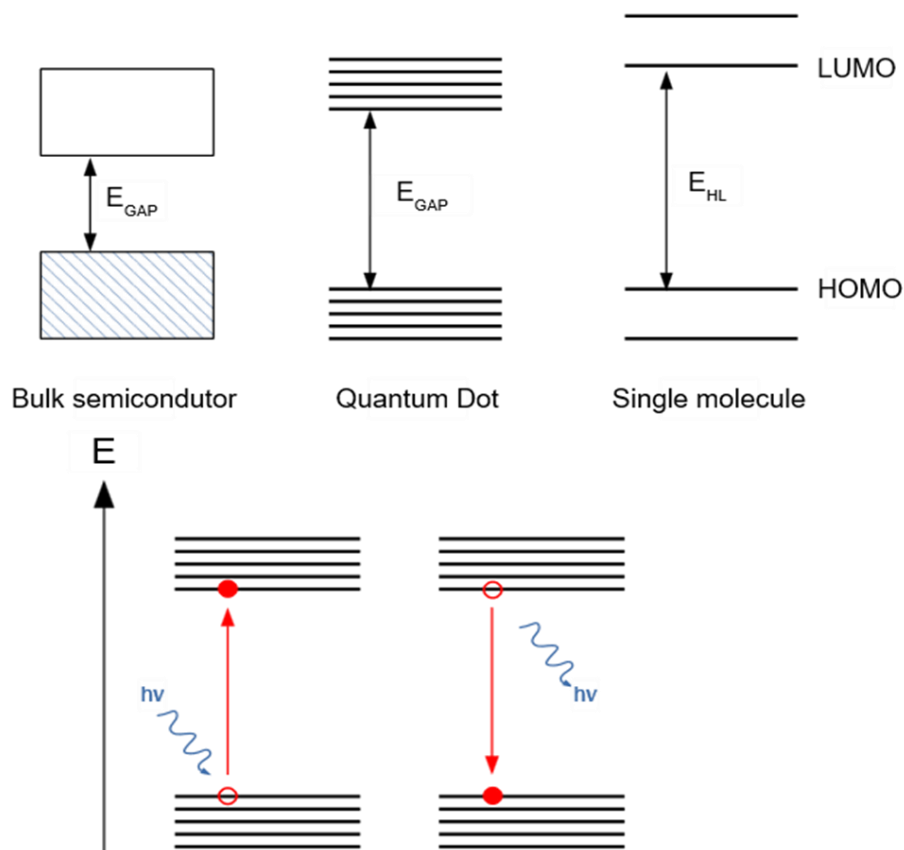
Fig. 14. Top panel: different band structures for bulk semiconductors, quantum dots, and single molecules. Bottom panel: photon absorption and emission mechanisms in QDs.

From Eq. (7), it can be observed that, as the particles get smaller, due to this quantum confinement phenomenon, the valence band and the conduction band lose their continuity, and band structure becomes similar to the one typical of the organic molecules, as shown in Fig. 14a. The spacing between two adjacent energy levels goes with the size of the QDs and is directly proportional to a^2.

Moreover, the width of the bandgap increases as the size decreases, and then the absorption wavelength can be tuned by changing the particle size.

QDs are widely employed for sensing purposes as fluorescent probes since it has been demonstrated that their fluorescence properties are sensitive to the presence of adsorbates of different nature.

QDs can be employed as an inorganic replacement to organic dyes [63] with two major advantages. First, they usually exhibit much narrower emission peaks [64]

whose position is tunable by changing their size, and, secondly, they are also less sensitive to photobleaching phenomena [63].

Different synthesis methods are available for the different types of QDs [22, 65, 66]. For instance, among the methods available for graphene QDs production, there are both some top-down approaches, such as oxidative cutting of the carbon fiber or acidic oxidation of coal, and bottom-up approaches like the glucose/fructose microwave-assisted hydrothermal synthesis or the hydrothermal treatment of nitrated pyrene in NaOH.

As far as Si QDs are concerned, the most common methods include laser ablation, non-thermal plasma synthesis, electrochemical etching, hydrothermal decomposition of organic precursors containing Si.

CdSe and CdTe QDs are instead usually synthesized by rapid injection of dymethilcadmium and chalcogenide sources into heated tri-n-octilphosphine oxide (TOPO), which result in the formation of a massive amount of CdE nuclei which consume almost totally the reactant and then prevent the subsequent growth.

Usually, after synthesis, QDs are embedded in a solid matrix and are therefore insulated from the rest of the environment: the most significant challenge when realizing QD-based sensors is to obtain this encapsulation without losing the sensing properties of the QDs, and different approaches may be employed.

One of the most common ways is the deposition of QDs by dip coating. For example, Zhang et al. [67] realized an ethanol and water vapor sensor based on Si-QDs deposited on the end of an optical fiber (OF) (see Fig. 15b) by simply dipping into a solution of the QDs itself and drying under environmental conditions. The sensor was interrogated through a blue diode laser, and the fluorescence spectra of the Si-QDs were then collected, showing an increase in its intensity when the sensor is exposed to water or ethanol vapor (see Fig. 15a).
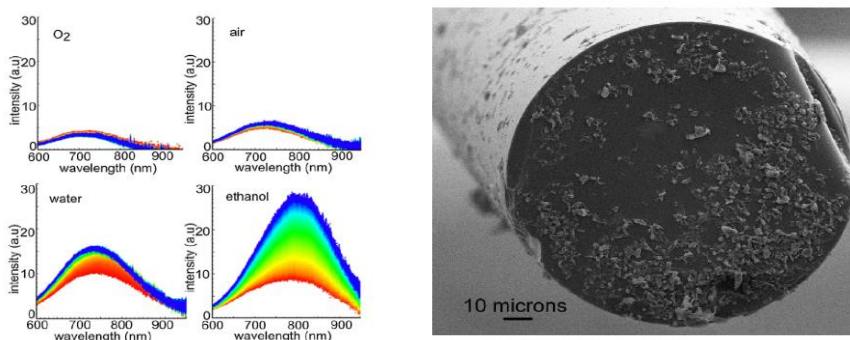
Fig. 15. a) Fluorescence spectra of the Si-QDs exposed to oxygen, air, water vapor, and ethanol vapor over 1h. b) SEM image showing Si-QDs at the end of an OF. Reproduced from [67]. Copyright 2013, with permission from Elsevier.

Wu et al. [68] realized a flexible glass surface acoustic wave (SAW) humidity sensor based on ZnO nanowires and graphene QDs (GQDs). First of all, a film of ZnO was deposited on the flexible glass employing DC sputtering using Zn as a target under a

mixed atmosphere of Ar/O$_2$. The sensor was then processed with UV photolithography and liftoff process to create the SAW resonator on the ZnO coated glass and eventually immersed in a solution of the ZnO nanowires and GQDs.

Yu et al. [69] realized a glucose sensor based on carbon quantum dots-glucose oxidase/cellulose acetate complex (CQDs-GOD/CA) immobilized by dip coating on the surface of an OF. A bare portion of the OF was immersed into a CQDs-GOD/CA precursor casting solution, then dried a 4 °C for slow removal of the solvent and leading to CQDs-GOD/CA complex sensitive film formation. The device's exposure to a glucose solution activates some enzymatic reactions that lead to the formation of hydrogen peroxide and a decrease in the QDs fluorescence intensity.

Sensors may also be produced encapsulating the QDs via a sol-gel process like in the work by Jorge et al. [70], where CdTe was dispersed into a Ru doped glass matrix to realize an oxygen concentration sensor based on the dynamic quenching of fluorescence of a ruthenium complex, such as Ru(bpy) and Ru(dpp).

In this case, the QDs were realized with a core-shell structure covering the CdTe core with a ZnS layer to ensure better stability of the optical properties and avoid some possible oxidation reactions. Moreover, these sensors also demonstrate that the intensity, wavelength, and width of the QDs luminescent peak are affected by the temperature so that they could be used for monitoring both oxygen concentration and temperature simultaneously.
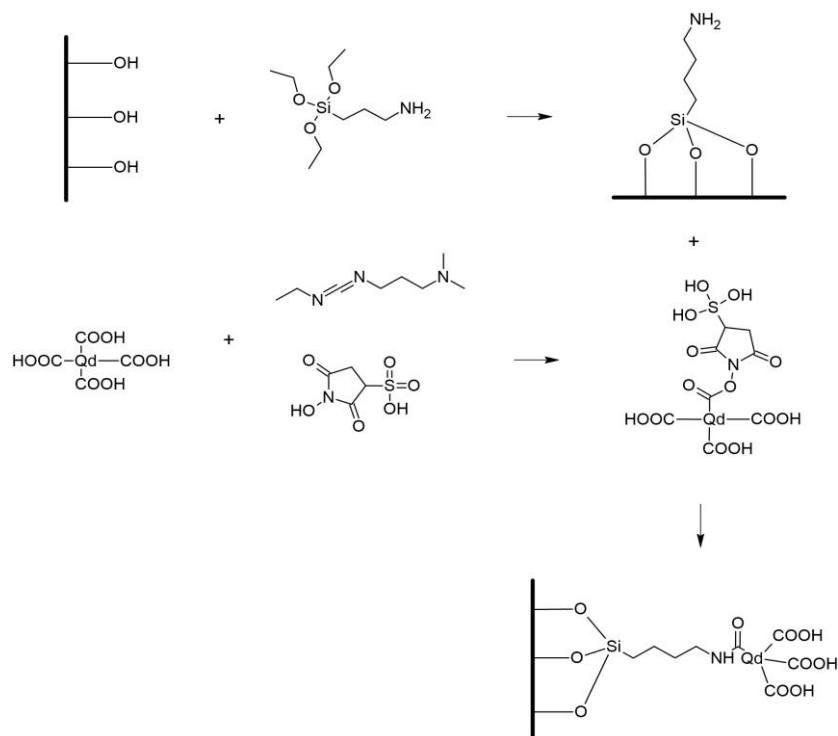
Fig. 16. Carboxylated QDs encapsulation on an OF surface via silanization and subsequent EDC/sulfo-NHS coupling reaction. Adapted from [71].

Zhao et al. [71], instead, exploited a 1-ethyl-3-(3-dimethylaminopropyl) carbodiimide hydrochloride/sulfo-N-hydroxy sulfosuccinimide (EDC/sulfo-NHS) coupling reaction to immobilize some CdSe/ZnS QDs with different sizes (and therefore different emission colors) functionalized with carboxylate groups on the surface of an OF and obtain a pH sensor.

The silica of the OF was first functionalized with 3-aminopropyltriethoxysilane (APTES) to obtain -NH_2 surface groups and then incubated in a solution of EDC/Sulfo-NHS and QDs overnight to obtain a condensation reaction between the amino and the carboxylic groups, as illustrated in Fig. 16.

The QD-COOH functionalized optical fiber was successfully employed as a pH probe as it was observed that the photoluminescence (PL) intensity of QDs increased linearly with the increase of pH. Also, a slight red-shift of the emission peak was observed as the pH was increased. Both these phenomena are likely to ionization of the QDs carboxyl ligand.

5 Conclusion and outlook

The selection of the most suitable material and the development of new ones pushing the limits of the actual performance is of paramount importance in the progress of sensors. While more traditional approaches are commonly used, a great activity in this field of research is ongoing and has much room ahead for development. To confirm this view, state-of-the-art glass/glass-ceramic materials for sensors were covered in this review alongside innovative approaches that leverage, e.g., glass/ceramic nano-materials, quantum dots, thin films. Although the field is vast, a strong effort in applying the most recent advancement in photonic materials emerges in the literature, indicating a clear path for development to reach more performing and innovative sensors. Indeed, from an economic point of view, the photonic sensors market is expected to garner $18 billion by 2021, registering a compound annual growth rate (CAGR) of 17.7% during the forecast period 2016-2021. Current data also confirm that the winning strategy in this field is based on new product launches (80%) [72]. Those facts testify to the tremendous economic drivers behind the need for new and more performing sensors to pave the way for better control in industrial processes even in harsh environments, better environmental protection, and more sensitive and effective biosensors. To this aim, the development of new or more performing materials, and glass-ceramics in particular, could represent a key enabling technology for the advancement of the photonic sensors' field. For this reason, more research and scientific efforts are required calling for a more interdisciplinary approach increasing the fruitful mutual exchanges between the materials science and the photonic communities.

References

1. Stronczek, M.: Glass-ceramics revolutionize exhaust gas sensors, https://www.schott.com/d/epackaging/8af058af-c66a-4399-83bc-92dcaffa40ad, last accessed 2021/06/18.

2. Advanced Ceramic Materials for Sensor Applications, https://www.frontiersin.org/research-topics/14727/advanced-ceramic-materials-for-sensor-applications, last accessed 2021/02/22.

3. Alemohammad, H.: Opto-mechanical Fiber Optic Sensors. 1st edn. Butterworth-Heinemann Elsevier Ltd, Oxford (2018).

4. Dong, X., Zhang, H., Liu, B., Miao, Y.: Tilted fiber Bragg gratings: Principle and sensing applications. Photonic Sensors 1(1), 6–30 (2011).

5. Ozcariz, A., Ruiz-Zamarreño, C., Arregui, F.J.: A comprehensive review: materials for the fabrication of optical fiber refractometers based on lossy mode resonance. Sensors 20(7), 1972 (2020).

6. Nikl, M.: Scintillation detectors for x-rays. Measurement Science and Technology 17(4), R37–R54 (2006).

7. Leonard, R.L., Johnson, J.A.: Scintillator Glasses. In: Musgraves, J.D., Hu, J., Calvez, F. (eds.) Springer Handbook of Glass, pp. 1555–1584. Springer, Cham (2019).

8. De Faoite, D., Hanlon, L., Roberts, O., Ulyanov, A., McBreen, S., Tobin, I., Stanton, K.T.: Development of glass-ceramic scintillators for gamma-ray astronomy. Journal of Physics: Conference Series 620, 012002 (2015).

9. Struebing, C., Chong, J.Y., Lee, G., Zavala, M., Erickson, A., Ding, Y., Wang, C.-L., Diawara, Y., Engels, R., Wagner, B., Kang, Z.: A neutron scintillator based on transparent nanocrystalline CaF_2:Eu glass ceramic. Applied Physics Letters 108(15), 153106 (2016).

10. Zheng, Z., Tong, Y., Wei, R., Hu, F., Sun, X., Guo, H.: Tb^{3+}-doped transparent $BaGdF_5$ glass-ceramics scintillator for X-ray detector. Journal of the American Ceramic Society 103(4), 2548–2554 (2020).

11. Kang, Z.T., Rosson, R., Barta, B., Han, C., Nadler, J.H., Dorn, M., Wagner, B., Kahn, B.: $GdBr_3$:Ce in glass matrix as nuclear spectroscopy detector. Radiation Measurements 48, 7–11 (2013).

12. Glebov, L.B., Nikonorov, N.V., Petrovsky, G.T.: Planar optical waveguides on glasses and glass-ceramic materials. In: SPIE ECO4 (The Hague '91), Glasses for Optoelectronics II, vol. 1513, pp. 56–70. Society of Photo-Optical Instrumentation Engineers, Bellingham, USA (1991).

13. Walker, R.G., Wilkinson, C.D.W., Wilkinson, J.A.H.: Integrated optical waveguiding structures made by silver ion-exchange in glass. 1: The propagation characteristics of stripe ion-exchanged waveguides; a theoretical and experimental investigation. Applied Optics 22(12), 1923–1928 (1983).

14. Gortych, J.E., Hall, D.G.: Fabrication of planar optical waveguides by K^+ ion exchange in BK7 glass. Optics Letters 11(2), 100–102 (1986).

15. Giallorenzi, T.G., West, E.J., Kirk, R., Ginther, R., Andrews, R.A.: Optical waveguides formed by thermal migration of ions in glass. Applied Optics 12(6), 1240–1245 (1973).

16. Chiasera, A., Vasilchenko, I., Dorosz, D., Cotti, M., Varas, S., Iacob, E., Speranza, G., Vaccari, A., Valligatla, S., Zur, L., Lukowiak, A., Righini, G.C., Ferrari, M.: SiO_2-P_2O_5-HfO_2-Al_2O_3-Na_2O glasses activated by Er^{3+} ions: From bulk sample to planar waveguide fabricated by rf-sputtering. Optical Materials 63, 153–157 (2017).

17. Almeida, R.M., Xu, J.: Sulfide glass optical waveguides prepared by sol-gel processing. In: Symposium on Integrated Optoelectronics, 2000, Sol-Gel Optics V, vol. 3943, pp. 58–66. Society of Photo-Optical Instrumentation Engineers, Bellingham, USA (2000).

18. Jestin, Y., Armellini, C., Chiappini, A., Chiasera, A., Ferrari, M., Goyes, C., Montagna, M., Moser, E., Nunzi Conti, G., Pelli, S., Retoux, R., Righini, G.C., Speranza, G.: Erbium activated HfO_2 based glass–ceramics waveguides for photonics. Journal of Non-Crystalline Solids 353(5–7), 494–497 (2007).

19. Miniscalco, W.J.: Erbium-doped glasses for fiber amplifiers at 1500 nm. Journal of Lightwave Technology 9(2), 234–250 (1991).

20. Zhang, Y., Nizamidin, P., Abudukeremu, H., Yimit, A.: Optical waveguide xylene gas sensor based on sodium dodecylbenzene sulfonate (SDBS)–TiO$_2$ film for detection at room temperature. Optical Materials Express 10(9), 2212–2226 (2020).

21. Han, Z., Lin, P., Singh, V., Kimerling, L., Hu, J., Richardson, K., Agarwal, A., Tan, D.T.H.: On-chip mid-infrared gas detection using chalcogenide glass waveguide. Applied Physics Letters 108(14), 141106 (2016).

22. Gaur, S.S., Singh, P.K., Gupta, A., Singh, R., Kumar, Y.: Synthesis and analysis of planar optical waveguides as pH sensors. Recent Innovations in Chemical Engineering 11(1), 40–44 (2018).

23. MacCraith, B.D., Ruddy, V., Potter, C., O'Kelly, B., McGilp, J.F.: Optical waveguide sensor using evanescent wave excitation of fluorescent dye in sol-gel glass. Electronics Letters 27(14), 1247–1248 (1991).

24. Horváth, R., Pedersen, H.C., Skivesen, N., Selmeczi, D., Larsen, N.B.: Optical waveguide sensor for on-line monitoring of bacteria. Optics Letters 28(14), 1233–1235 (2003).

25. Seiyama, T., Kato, A., Fujiishi, K., Nagatani, M.: A new detector for gaseous components using semiconductive thin films. Analytical Chemistry 34(11), 1502–1503 (1962).

26. Touidjen, N.H., Bendahmane, B., Lamri Zeggar, M., Mansour, F., Aida, M.S.: SnO$_2$ thin film synthesis for organic vapors sensing at ambient temperature. Sensing and Bio-Sensing Research 11(1), 52–57 (2016).

27. Salman, S.H., Shihab, A.A., Kh. Elttayef, A.-H.: Design and construction of nanostructure TiO$_2$ thin film gas sensor prepared by R.F magnetron sputtering technique. Energy Procedia 157, 283–289 (2019).

28. Salah, G., Telia, A., Boukaous, C.: Fabrication of ZnO thin film based humidity sensor with fast response by sol-gel associated to spin coating method. In: 2015 3rd International Conference on Control, Engineering & Information Technology (CEIT), pp. 1–4. Institute of Electrical and Electronics Engineers, Tlemcen, Algeria (2015).

29. Mourzina, Y., Schöning, M.J., Schubert, J., Zander, W., Legin, A.V., Vlasov, Y.G., Kordos, P., Lüth, H.: A new thin-film Pb microsensor based on chalcogenide glasses. Sensors and Actuators B: Chemical 71(1–2), 13–18 (2000).

30. Diyatmika, W., Chu, J.P., Kacha, B.T., Yu, C.-C, Lee, C.-M.: Thin film metallic glasses in optoelectronic, magnetic, and electronic applications: A recent update. Current Opinion in Solid State and Materials Science 19(2), 95–106 (2015).

31. Xian, H.J., Cao, C.R., Shi, J.A., Zhu, X.S., Hu, Y.C., Huang, Y.F., Meng, S., Gu, L., Liu, Y.H., Bai, H.Y., Wang, W.H.: Flexible strain sensors with high performance based on metallic glass thin film. Applied Physics Letters 111(12), 121906 (2017).

32. Gopalan, K.K., Janner, D., Nanot, S., Parret, R., Lundeberg, M.B., Koppens, F.H.L., Pruneri, V.: Mid-infrared pyroresistive graphene detector on LiNbO$_3$. Advanced Optical Materials 5(4), 1600723 (2017).

33. Kashyap, R.: Fiber Bragg Gratings. 2nd edn. Academic Press Elsevier Ltd, Cambridge, MA, USA (2010).

34. Fan, Z., Diao, X., Hu, K., Zhang, Y., Huang, Z., Kang, Y., Yan, H.: Structural health monitoring of metal-to-glass–ceramics penetration during thermal cycling aging using femto-laser inscribed FBG sensors. Scientific Reports 10(1), 12330 (2020).

35. Chiavaioli, F., Janner, D.: Fiber optic sensing with lossy mode resonances: applications and perspectives. Journal of Lightwave Technology 39(12), 3855–3870 (2021).

36. Li, Z., Bao, Q., Zhu, J., Ruan, X., Dai, Y.: Generation of leaky mode resonance by metallic oxide nanocoating in tilted fiber-optic gratings. Optics Express 28(7), 9123–9135 (2020).

37. Consales, M., Quero, G., Spaziani, S., Principe, M., Micco, A., Galdi, V., Cutolo, A., Cusano, A.: Metasurface-enhanced lab-on-fiber biosensors. Laser & Photonics Reviews 14(12), 2000180 (2020).

38. Lao, J., Sun, P., Liu, F., Zhang, X., Zhao, C., Mai, W., Guo, T., Xiao, G., Albert, J.: "In situ plasmonic optical fiber detection of the state of charge of supercapacitors for renewable energy storage. Light: Science & Applications 7(1), 34 (2018).

39. Liu, Y., Liang, B., Zhang, X., Hu, N., Li, K., Chiavaioli, F., Gui, X., Guo, T.: Plasmonic fiber-optic photothermal anemometers with carbon nanotube coatings. Journal of Lightwave Technology 37(13), 3373–3380 (2019).

40. Chiavaioli, F., Giannetti, A., Baldini, F.: From refractometry to biosensing with optical fibres. In: Del Villar, I., Matias, I.R. (eds.) Optical fibre sensors: fundamentals for development of optimized devices, pp. 331–366. John Wiley & Sons, Inc., Hoboken (2021).

41. Gonzalez-Valencia, E., Del Villar, I., Torres, P.: Bloch waves at the surface of a single-layer coating D-shaped photonic crystal fiber. Optics Letters 45(9), 2547–2550.

42. Socorro-Lleránoz, A.B., Santano, D., Del Villar, I., Matias, I.R.: Trends in the design of wavelength-based optical fibre biosensors (2008–2018). Biosensors and Bioelectronics: X 1, 100015 (2019).

43. Chiavaioli, F., Zubiate, P., Del Villar, I., Zamarreño, C.R., Giannetti, A., Tombelli, S., Trono, C., Arregui, F.J., Matias, I.R., Baldini, F.: Femtomolar detection by nanocoated fiber label-free biosensors. ACS Sensors 3(5), 936–943 (2018).

44. Kosiel, K., Koba, M., Masiewicz, M., Śmietana, M.: Tailoring properties of lossy-mode resonance optical fiber sensors with atomic layer deposition technique. Optics & Laser Technology 102, 213–221 (2018).

45. Wei, Z., Sun, L., Liu, J., Zhang, J.Z., Yang, H., Yang, Y., Shi, L.: Cysteine modified rare-earth up-converting nanoparticles for *in vitro* and *in vivo* bioimaging. Biomaterials 35(1), 387–392 (2014).

46. Zhao, P., Zhu, Y., Yang, X., Shen, J., Jiang, X., Zong, J., Li, C.: Multifunctional MnO_2 nanosheet-modified $Fe_3O_4@SiO_2/NaYF_4$:Yb, Er nanocomposites as novel drug carriers. Dalton Transactions 43(2), 451–457 (2014).

47. Guo, K., Li, M., Fang, X., Luoshan, M., Bai, L., Zhao, X.: Performance enhancement in dye-sensitized solar cells by utilization of a bifunctional layer consisting of core-shell β-$NaYF_4$:Er^{3+}/Yb^{3+}@SiO_2 submicron hexagonal prisms. Journal of Power Sources 249, 72–78 (2014).

48. Jiang, S., Guo, H., Wei, X., Duan, C., Yin, M.: Enhanced upconversion in Ho^{3+}-doped transparent glass ceramics containing $BaYbF_5$ nanocrystals. Journal of Luminescence 152, 195–198 (2014).

49. Dey, R., Rai, V.K.: Yb^{3+} sensitized Er^{3+} doped La_2O_3 phosphor in temperature sensors and display devices. Dalton Transactions 43(1), 111–118 (2014).

50. Li, X., Yuan, S., Hu, F., Lu, S., Chen, D., Yin, M.: Near-infrared to short-wavelength upconversion temperature sensing in transparent bulk glass ceramics containing hexagonal $NaGdF_4$: Yb^{3+}/Ho^{3+} nanocrystals. Optical Materials Express 7(8), 3023–3033 (2017).

51. Zhong, J.S., Chen, D.Q., Peng, Y.Z., Lu, Y.D., Chen, X., Li, X.Y., Ji, Z.G.: A review on nanostructured glass ceramics for promising application in optical thermometry. Journal of Alloys and Compounds 763, 34–48 (2018).

52. Chen, D., Liu, S., Li, X., Yuan, S., Huang, P.: Upconverting luminescence based dual-modal temperature sensing for Yb^{3+}/Er^{3+}/Tm^{3+}: YF_3 nanocrystals embedded glass ceramic. Journal of the European Ceramic Society 37(15), 4939–4945 (2017).

53. Rami Reddy, B., Kamma, I., Kommidi, P.: Optical sensing techniques for temperature measurement. Applied Optics 52(4), B33–B39 (2013).

54. Jiang, S., Zeng, P., Liao, L., Tian, S., Guo, H., Chen, Y., Duan, C., Yin, M.: Optical thermometry based on upconverted luminescence in transparent glass ceramics containing $NaYF_4:Yb^{3+}/Er^{3+}$ nanocrystals. Journal of Alloys and Compounds 617, 538–541 (2014).

55. Mukhopadhyay, L., Rai, V.K.: Upconversion based near white light emission, intrinsic optical bistability and temperature sensing in $Er^{3+}/Tm^{3+}/Yb^{3+}/Li^+:NaZnPO_4$ phosphors. New Journal of Chemistry 41(15), 7650–7661 (2017).

56. León-Luis, S.F., Rodríguez-Mendoza, U.R., Lalla, E., Lavín, V.: Temperature sensor based on the Er^{3+} green upconverted emission in a fluorotellurite glass. Sensors and Actuators B: Chemical 158(1), 208–213 (2011).

57. Chen, S.Y.Z., Song, W.H., Cao, J.K., Hu, F.F., Guo, H.: Highly sensitive optical thermometer based on FIR technique of transparent $NaY_2F_7:Tm^{3+}/Yb^{3+}$ glass ceramic. Journal of Alloys and Compounds 825, 154011 (2020).

58. Chen, D., Xiang, W., Liang, X., Zhong, J., Yu, H., Ding, M., Lu, H., Ji, Z.: Advances in transparent glass–ceramic phosphors for white light-emitting diodes—A review. Journal of the European Ceramic Society 35(3), 859–869 (2015).

59. Chen, D., Zhou, Y., Xu, W., Zhong, J., Huang, P.: Persistent and photo-stimulated luminescence in Ce^{3+}/Cr^{3+} activated $Y_3Al_2Ga_3O_{12}$ phosphors and transparent phosphor-in-glass. Journal of Materials Chemistry C 4(48), 11457–11464 (2016).

60. Xu, J., Ueda, J., Kuroishi, K., Tanabe, S.: Fabrication of Ce^{3+}–Cr^{3+} co-doped yttrium aluminium gallium garnet transparent ceramic phosphors with super long persistent luminescence. Scripta Materialia 102, 47–50 (2015).

61. Fedorov, P.P., Luginina, A.A., Popov, A.I.: Transparent oxyfluoride glass ceramics. Journal of Fluorine Chemistry 172, 22–50 (2015).

62. Lin, G., Pan, H., Dai, Y., He, F., Chen, D., Cheng, Y., Jiang, X., Zhang, L., Qiu, J., Zhao, Q.: Formation of Si nanocrystals in glass by femtosecond laser micromachining. Materials Letters 65(23–24), 3544–3547 (2011).

63. Murphy, C.J.: Peer reviewed: optical sensing with quantum dots. Analytical Chemistry 74(19), 520 A–526 A (2002).

64. Resch-Genger, U., Grabolle, M., Cavaliere-Jaricot, S., Nitschke, R., Nann, T.: Quantum dots versus organic dyes as fluorescent labels. Nature Methods 5(9), 763–775 (2008).

65. Klimov, V.I.: Semiconductor and metal nanocrystals: synthesis and electronic and optical properties. 1st edn. CRC Press, Boca Raton (2003).

66. Kalluri, A., Debnath, D., Dharmadhikari, B., Patra, P.: Chapter twelve - graphene quantum dots: synthesis and applications. Methods in Enzymology 609, 335–354 (2018).

67. Zhang, Z.H., Lockwood, R., Veinot, J.G.C., Meldrum, A.: Detection of ethanol and water vapor with silicon quantum dots coupled to an optical fiber. Sensors and Actuators B: Chemical 181, 523–528 (2013).

68. Wu, J., Yin, C., Zhou, J., Li, H., Liu, Y., Shen, Y., Garner, S., Fu, Y., Duan, H.: Ultrathin glass-based flexible, transparent, and ultrasensitive surface acoustic wave humidity sensor with ZnO nanowires and graphene quantum dots. ACS Applied Materials & Interfaces 12(35), 39817–39825 (2020).

69. Yu, S., Ding, L., Lin, H., Wu, W., Huang, J.: A novel optical fiber glucose biosensor based on carbon quantum dots-glucose oxidase/cellulose acetate complex sensitive film. Biosensors and Bioelectronics 146, 111760 (2019).

70. Jorge, P.A.S., Mayeh, M., Benrashid, R., Caldas, P., Santos, J.L., Farahi, F.: Applications of quantum dots in optical fiber luminescent oxygen sensors. Applied Optics 45(16), 3760–3767 (2006).

71. Zhao, F., Kim, I., Kim, J.: Fabrication of the optical fiber pH sensor based on CdSe/ZnS quantum dot. Journal of Nanoscience and Nanotechnology 14(8), 5650–5653 (2014).

72. https://www.alliedmarketresearch.com/photonics-sensor-market, last accessed 2021/06/30.